EXTRACTING CRATER SHAPE INFORMATION FROM NARROW ANGLE CAMERA DTMS. T. J. Thompson[1], P. Mahanti[1], and M. S. Robinson[1] and the LROC Team, [1]Lunar Reconnaissance Orbiter Camera Science Operations Center, School of Earth and Space Exploration, Arizona State University, 1100 S. Cady, Tempe, AZ 85287 (tjthomp9@asu.edu).

Introduction: Digital Terrain Models (DTMs) of the lunar surface derived from stereo images [1] obtained by the Lunar Reconnaissance Orbiter Camera (LROC) Narrow Angle Camera (NAC) enable the detailed study of areas of interest. NAC DTMs have pixel scales of 2 to 5 m, compared to 100 meter pixel scale for the Wide Angle Camera (WAC) [2] GLD100. Thus sites with NAC DTMs allow the study of landforms at the scale of several meters (exploration relevant scales).

Impact crater density is related to surface age [3,4]. Fresh craters with sharp rims, steep inner wall slopes, and visible ejecta degrade to craters with broad or indistinguishable rims, shallow sloped walls, and no ejecta [5-9]. The processes whereby craters degrade over time include micrometeorite bombardment, moonquakes, and direct obliteration from subsequent impact [10-12].

Three dimensional shape information provides insight into crater age, degradation rate, and material properties [13-19]. But, with so many craters existing within any given image, a detailed study of their topography requires some automation to increase efficiency in multi-site comparisons (thousands of craters per site). We developed a procedure to rapidly identify craters, classify their degradation state, and automatically extract shape information enabling new quantitative landform analysis (**Fig. 1**).

Methods: Craters were identified in QGIS [20] and ArcGIS CraterTools [21] software. Topography extraction, rim identification and adjustment, qualitative classification, and quantitative metrics were completed in MATLAB.

Crater identification. LROC NAC [22] orthophotos, DTMs [1], and slope maps were downloaded for the Apollo 16 and Apollo 17 sites from the LROC archival site (http://lroc.sese.asu.edu/archive). QGIS software was used to compute hillshade maps to aid in crater identification. First, grids were generated for both the small size limit (diameter = 30 m) and maximum size for the study (diameter = 300 m) to guide digitization; grids were rendered semi-transparent overlaying the imagery. Then, the image was scrolled while cycling the slope, hillshades, and orthophotos from which the analyst identified craters. Craters were digitized as polygons using a click and drag circle tool in QGIS or a 3 point rim selection in ArcGIS [21]. Two or more people made multiple passes over the area in the digitization process to cross-check crater identifications.

Crater shape extraction. The shaperead and geotifread functions in MATLAB's map toolbox (https://www.mathworks.com/products/mapping.html) allow shapefiles and GeoTIFF files to be imported into a workspace as structures and matrices. For each feature (crater polygon) in the shapefile, the latitude-longitude pair defining each vertex in the polygon is intersected with the underlying raster, and the inner shape is filled to generate a mask layer (1 inside the crater, 0 outside). The mean row and column index of mask value 1 pixels gives the crater center index. An approximate crater radius is derived from the mean of the vertex coordinates defining the crater center and the mean distance from the center to surrounding vertices. The script crops out a rectangle three times the crater diameter in x and y dimensions from imagery and topography layers for use in later classification and calculations. Since the imagery and DTM overlay perfectly, the indices are equivalent for both layers. Several other parameters such as the central latitudes and longitudes, and a crater mask are also stored in the structure describing each crater. There is one structure containing the variables for each individual crater at this stage. The data in each crater structure includes cropped imagery, topography, central latitude-longitude values, and initialized values for degradation state, and presence or absence of a central feature.

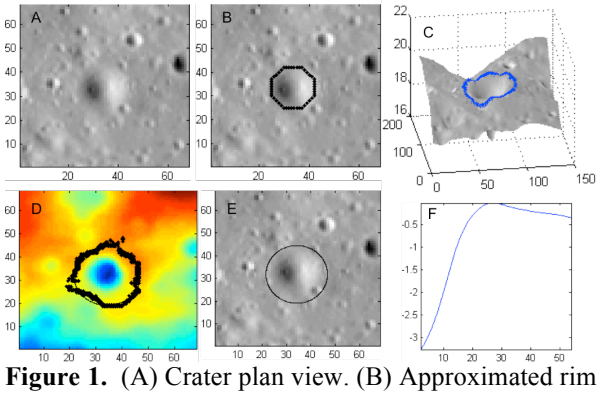

Figure 1. (A) Crater plan view. (B) Approximated rim in black. (C) Rim on 3d surface. (D) Rim positions (black dots) from azimuthal profile. (E) Parameterized fit circle. (F) Radial crater profile.

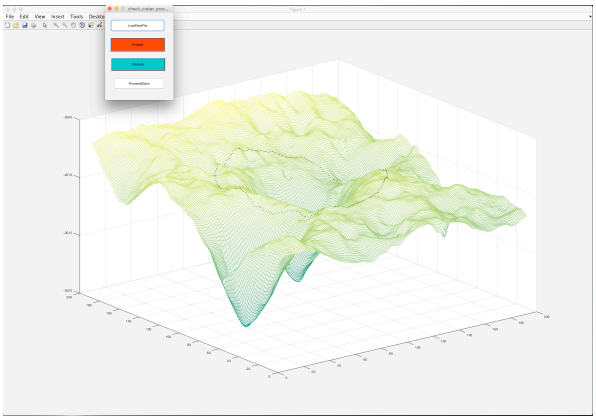

Figure 2. Rim position interface. A mesh of the topography with the rim position (blue dots) are displayed. The user has the option of manually dilating or contracting the rim positions.

Semi-automated rim identification. The fraction of crater radius (0R at crater center, 1R at crater rim) allows comparison between larger and smaller craters. One script generates an initial rim fit using the digitized polygon data as a guide. The baseline topography is subtracted and a rim position is isolated at 1 degree radial increments from the crater center. Next, a circle is fit to the azimuthally stacked rim positions. The fit circle describing the crater rim may then be interactively dilated or contracted by the user (**Fig. 2**) to correct for any peculiarities in the calculation from the irregular landscape or craters which failed automated processing.

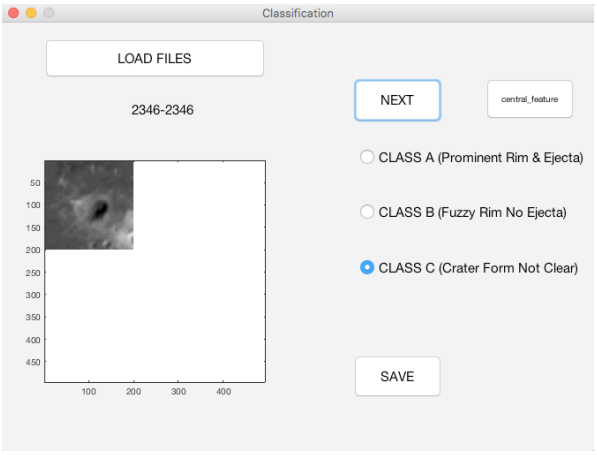

Figure 1. Interface for qualitative classification and central feature identification.

Qualitative classification method. Certain features of crater shape change with degradation over time. These features include the sharpness of the rim, the presence of visible ejecta, and the steepness of interior slopes [5-9]. Thus a qualitative relative freshness index separates craters into classes (A for freshest, B intermediate, C degraded) which we apply to our dataset to compare to shape metrics [23]. Given the thousands of craters in the 30 – 300 m size range of the sites, we generated a MATLAB tool that lets the user go crater by crater and visually classify the crater by degradation state (**Fig. 3**). The script loads and displays a crater, allowing the user to select the appropriate degradation state and flag if the crater has a central feature. This script makes the qualitative classification of all the crater degradation states efficient and systematic.

Radial profile calculations. After the crater radius is determined, other morphologic parameters are logged along each azimuthal vector at a specified distance interval. Elevations, slopes, and curvatures are calculated along fractions of the radius and compared across craters.

Summary: We developed a procedure using different software tools and scripts to rapidly and accurately classify craters and extract their topography from NAC DTMs. The methods outlined here were used to obtain a preliminary comparison of crater morphology across the Apollo sites [24,25]. With modification, this procedure may be applied to the study of other landforms.

References:

[1] Henriksen M.R. et al. (2017) *Icarus,* 283, 122-137. [2] Scholten F. et al. (2012) *JGR*, 117, E00H17. [3] Neukum G., et al. (1975), *The Moon,* 12, 201-229. [4] Marcus, A.H. (1970), *JGR,* 75, 4977-4984. [5] Trask N.J. (1967) *Icarus*, 6, 270-276. [6] Florensky, C., et al. (1976), *Earth, Moon, and Planets,* 16, 59-70. [7] Bazilevskiy, A., and V. Popovich (1979), *Intl. Geol. Rev,* 21, 277-280. [8] Fassett, C. I., and B. J. Thomson (2014), *JGR,* 119, 2255-2271. [9] Craddock, R.A. (2000), *JGR,* 105, 20387-20401. [10] Soderblom, L.A. (1970), *JGR,* 75, 2655-2661. [11] McGill, G.E. (1974), *Icarus,* 21, 437-447. [12] Schultz P., and D. Gault (1977), *PLPSC,* 2845-2862. [13] Bray, V.J. et al. (2008), *Met. Planet. Sci.,* 43, 1979-1992. [14] De Hon R.A. (1982), *PLPSC,* 639-650. [15] Head, J.W. (1976), *PLPSC,* 2913-2929. [16] Pike R. (1981) *PLPSC,* 845-847. [17] Shoemaker, E.M. (1965) in: *The Nature of the Lunar Surface*. [18] Smith, E.I., and J.A. Hartnell (1978), *The Moon and the Planets* 19, 479-511. [19] Croft, S.K (1978), *PLPSC,* 3711-3733. [20] QGIS Dev. Team, (2011), *Open Source Geospatial Foundation Project*. [21] Kneissl, T., et al. (2011), *PSS,* 59, 1243-1254. [22] Robinson, M.S., et al. (2010). *Space Sci. Rev.,* 150, 81-124. [23] Basilevsky, A., et al. (2014), *PSS,* 92, 77-87. [24] Mahanti, P., et al. (2017) *PLPSC*. [25] Mahanti, P. et al. (2017) *Icarus* (in revision).